

**Final assessment for the white paper call
Number of well-measured type Ia Supernovae**

*N. Regnault, Ph. Gris
September 21 2018*

Contents

1 Key design elements	1
1.1 Requirements on SN sampling	2
1.2 SN samples	3
1.3 Metrics	4
2 Method	4
2.1 Deep Drilling fields	4
2.2 Wide Fast Deep	6
3 Overview of observing strategies	7
3.1 Available strategies	7
3.2 Key properties	7
3.2.1 WFD	7
3.2.2 DDF	7
4 Results: Number of well-measured type Ia supernovae	9
4.1 WFD	9
4.2 DD	9
5 New proposals	12
5.1 DDF observing strategy	12
5.2 altsched rolling 80/20	16
5.3 altsched rolling 75/25	16
5.4 Adding a simple metric for SN in OpSim/SLAIR	16
6 Conclusion	16
A Derivation of formula 2	18
B DDF plots	18

1 Key design elements

SN cosmology is systematics-limited. Increasing the statistics in the Hubble diagram must be coupled with (1) advances in the measurement of the SN distances (i.e. a control at the per-mil level of the photometry and survey flux calibration, and possibly a 3-parameter SN standardization technique) (2) a better control of the SN astrophysical environment and its potential impacts on the SN light curves and distances (local host properties, absorption) (3) a

better control of the SN diversity (SN Ia sub-populations, population drift with redshift) (4) a precise determination of the survey selection function (SN identification, residual contamination by non-SN Ia's as a function of redshift).

Access to spectroscopy will not scale with the large amount of SNe LSST will deliver. About 10% of LSST SNe will benefit from a live spectrum. Securing spectroscopic host redshifts for the full LSST sample using the fiber spectrographs available in the southern hemisphere is challenging – although doable. As a consequence, all the studies listed above, in particular SN Ia identification and the standardization of SN luminosity distances will rely on the supernova light curves only. Obtaining high quality SN light curves is therefore a key design point of the SN survey. The average quality of the SN light curves depends exclusively on the observing strategy.

Furthermore, spectroscopic time being scarce, we cannot afford to waste it. This means that all transients identified spectroscopically, around peak luminosity, as SNe Ia, *must* eventually have light curves of sufficient quality to end up in the Hubble diagram. This puts another requirement on the regularity and predictability of the observing strategy.

Since light curve quality is at the core of the design of the LSST SN survey, we propose to adopt as our main metric, the size and redshift extent of the subset of well sampled SNe Ia. We define in the next section what we mean by “well-sampled”.

Four key facets of observing strategy that have an impact on the number and on the quality of well-measured supernovae may be identified: *a regular cadence* (typical values: three to four days) is important to get well-sampled light curves ; minimal inter-night gaps are mandatory to keep a high detection efficiency of the supernovae; the *season length* has an impact on the total number of supernovae that may be collected ; 170 to 180 days are values of interest for supernova science; *depth* quantified by m5, the five-sigma depth, which is the magnitude corresponding to a flux with a signal-to-noise ratio (SNR) equal to 5. Since only light curve points of well-measured supernovae with $\text{SNR} > 5$ are considered, m5 has an impact on the redshift limit of observation (photostatistic limit); *spatial coverage and uniformity* which has an impact both on the wide and on the deep surveys; it may be interesting to observe deep fields evenly distributed in Ra (and Galactic/Ecliptic planes avoided) so as to search for anisotropies using individual Hubble diagrams.

1.1 Requirements on SN sampling

Light curves are the essential ingredient to (1) measure standardized luminosity distances and (2) photometrically identify SNe Ia from their full light curve. This drives a series of requirements which we summarize below.

1. each SN must have good quality measurements in at least three bands. We need two bands, covering the restframe B and V region, to constrain the restframe color of the SN. We need to provision an additional band (redder than restframe V), to enable next generation standardization techniques, that will likely rely on two restframe colors.
2. the follow-up of each supernova must be good enough in the observer-frame bands that correspond to the B - and V -restframe spectrum ($3800 \text{ \AA} < \lambda < 7000 \text{ \AA}$). At high-redshift,

in particular, one should avoid relying on the *UV* restframe region to derive a distance, given the high intrinsic dispersion of SN Ia at those wavelengths.

3. we require the light curve shape to be well sampled in the (restframe) phase interval $[-10; +30]$ days, with at least five visits before peak (each of those visits in any of the eligible band), and ten visits after peak. To obtain this in the lower redshift region of the Hubble diagram, one requires an observer-frame cadence of 4 days. At higher redshifts redshifts (DDF fields), this requirement may be slightly relaxed. However, since we are going to rely almost exclusively on photometric identification, it is essential to secure a tight sampling of the SN color evolution at all redshift.
4. we require that the photon noise contribution to the distance measurement is subdominant w.r.t. the intrinsic dispersion of the SNe (after standardization). There are several ways to quantify this. With today’s standardization techniques, the SN standardized distance modulus is:

$$\mu = m_B^* + \alpha X_1 - \beta C - \mathcal{M} \quad (1)$$

where m_B^* is the peak brightness in restframe B , X_1 characterize the lightcurve width, and C is an estimate of the restframe color $B - V$. α , β and \mathcal{M} are global parameters, fit along with the cosmology. If the light curve is correctly sampled (see point above), the propagation of the measurement uncertainties affecting m_B^* , X_1 and C is dominated by the contribution of σ_C . (since $\beta \sim 3$). In practice, requiring $\sigma_C < 0.04$ ensures that $\sigma\mu < 0.1$, below the intrinsic dispersion in the Hubble diagram, after standardization.

This last requirement may be re-expressed as a requirement on the signal-to-noise on the light-curve amplitude in each band. Indeed, if we fit a light curve model $L(t) = A \times \ell(t)$ one can show that:

$$\text{SNR}_{\text{band}} = \sum_i 5 \times (f_{i|5}^{-2} L_i^2)^{1/2} \quad (2)$$

where $5 - \sigma$ is the limiting flux of each visit $f_{i|5}$. This metrics is simpler in the sense that it does not require to use a SN light curve fitter. One just need lightcurve templates and the limiting magnitudes of each visit – given in the cadence databases. In practice, using $\text{SNR}_g >$ (for z_j), and $\text{SNR}_r >$, $\text{SNR}_i >$ and $\text{SNR}_z >$ allows to fulfill the requirement on color resolution above.

1.2 SN samples

The SN sample usable for cosmology can be defined from the light curve requirements listed in the previous section. The key quantity is the redshift limit, z_{lim} , beyond which one starts loosing events because of poor sampling. This “redshift-limit” is not a detectability limit. It is the redshift value beyond which we start losing a fraction of the events, because their photometric follow-up does not match the requirements listed in the previous section.

The definition of the redshift limit depends on the intrinsic luminosity of the supernova considered. SN Ia luminosities can be parametrized using two parameters, e.g. lightcurve width (X_1) and SN restframe B-V color at peak (C). As shown on figure 1, the SN distribution in

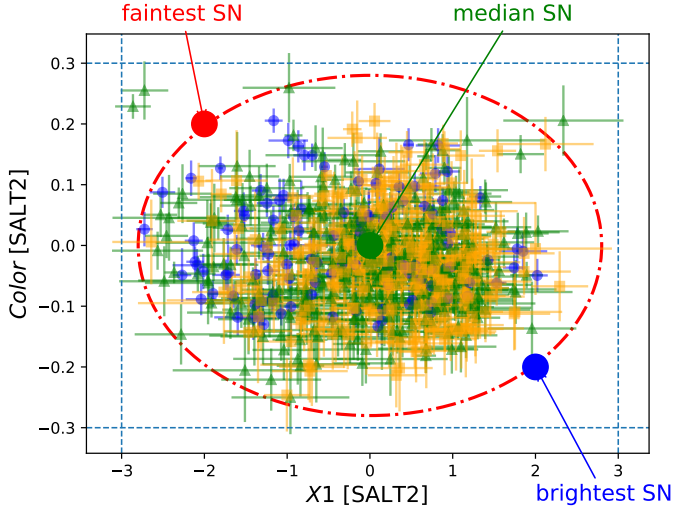


Figure 1: JLA supernovae the (X_1, Color) parameter space – (blue: nearby, green: SDSS, orange: SNLS). The large dots indicate the position of the faint, median and bright fiducial SNe used for the cadence analyses.

this parameter space is compact and more than 95% of the statistics can be enclosed in a tight ellipse.

On the same figure, we have represented three fiducial SNe of particular interest: the red dot represents the faintest SN in this region of the parameter space ($X_1 = -2, C = 0.2$), the green dot and blue dots show the average ($X_1 = 0, C = 0$) and brightest SN ($X_1 = 2, C = -0.2$) respectively.

We can define the redshift limit z_{faint} as the limit beyond which the faintest fiducial SN no longer passes the light curve requirements. By doing this, we ensure that all SNe that live in the fiducial (X_1, C) parameter space and are below z_{faint} do pass our light curve requirements. z_{faint} defines a *redshift-limited sample* whose selection function does not depend on the SN properties.

We can also define a similar limit, using the median supernova, instead of the faint one. This defines a SN sample whose upper redshift bins are affected by a selection bias, which must be determined using a simulation – which itself depends on our knowledge of the SN luminosity distribution at those redshifts. The uncertainty affecting the determination of the selection function generally limits the usefulness of the redshift bins affected by a selection bias. Since the selection function is generally symmetric around its 50% point, the size of the sample limited by z_{med} gives a good approximation of the total number of LSST SNe that will have precise distances.

1.3 Metrics

We propose to use as our primary metrics the size and depth of the subset of well sampled SNe. More precisely, we estimate, for each cadence, the following quantities:

- the sample redshift limit, z_{faint} defined above, and the number of well sampled supernovae below the redshift limit $N_{z < z_{\text{faint}}}$
- the redshift z_{med} at which the median supernova defined above no longer passes the signal-to-noise requirements, and the number of well-sampled supernovae below this redshift, $N_{z < z_{\text{med}}}$.

The former give an assessment of the size and depth of the redshift limited sample, i.e. the sample of supernovae usable for cosmology, and whose selection function is extremely easy to determine. The latter gives an assessment of the size and depth of the sample of SNe that will have precise distances.

2 Method

2.1 Deep Drilling fields

The DDF observations involve a small number of fields and $O(10^4)$ SNe. The list of DDF simulated is given in table 1 and on figure 2. The location of four DDF (referred to as reference fields in the following: COSMOS, XMM-LSS, CDFS and ELAIS-S1) has already been chosen by the project. The number of considered DDF ranges from 4 to 9.

Field name	OpSim ID	Ra (deg)	Dec(deg)	Observing strategies
COSMOS	2786	150.36	2.84	All
XMM-LSS	2412	34.39	-5.09	All
CDFS	1427	53.00	-27.44	All
ELAIS-S1	744	0.	-45.52	All
SPT DEEP	290	349.39	-63.32	All except feature*
DDF_820	820	119.55	-43.37	kraken_2035
DDF_858	858	187.62	-42.49	kraken_2035
DDF_1200	1200	176.63	-33.15	kraken_2035
DDF_2689	2689	201.85	0.93	kraken_2035

Table 1: List and location of Deep Drilling Fields observed.

DDF observations are composed of sequences of 96 visits (in a row) in r,g,i,z,y bands (namely 20,10,20,26,20 visits). This corresponds to a total observing time of about one hour and few minutes if filter changes, slew times and telescope overheads are taken into account.

The strategy to estimate the number of well-measured type Ia supernovae may be summarized in four steps: (1) light curves are simulated and fitted using observations of a given cadence;

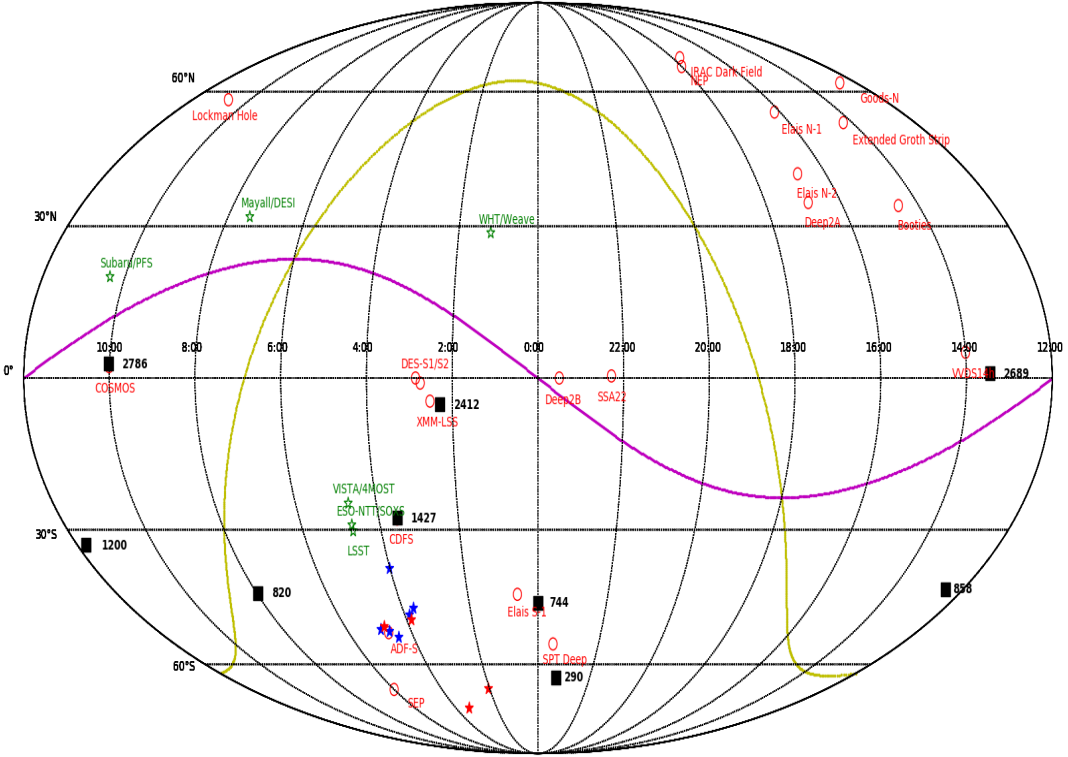


Figure 2: Location of the Deep Drilling fields observed (black squares). Deep fields observed by previous surveys (red circles) and potential candidates for spectroscopic follow-up (green stars) are also mentioned. Yellow and magenta lines represent the Galactic and Ecliptic planes, respectively. Blue and red stars indicate potential deep field locations for EUCLID and WFIRST, respectively.

(2) selection criteria are applied to get high-quality supernovae; (3) the resulting observing efficiency curves are then convolved with a production rate [1] so as to estimate the number of well-measured type Ia supernovae that may be collected by LSST given an observing strategy.

Table 2 summarizes the parameter used in SN simulations. The selection of a sample of well-measured type Ia supernovae is done in two steps. A sample of observable supernovae is selected by requiring light curves to have $ph_{min} \leq -5$ and $ph_{max} \geq 20$ (where ph_{min} and ph_{max} are the minimal and maximum phases of the LC points, respectively). For each supernovae in this reference sample, additional selection criteria are applied:

- $N_{bef} \geq 4$ and $N_{aft} \geq 10$ where N_{bef} and N_{aft} are the number of LC points (with $\text{SNR} \geq 5$) before and after T_0 .
- $\sigma_c \leq 0.04$ where σ_c is the error on the c parameter estimated from the fit of the light curve.

The season length which depends on the redshift is estimated using the supernovae of the reference sample.

Parameter	Range
(X_1, c)	$(-2.0, 0.2), (0.0, 0.0), (2.0, -0.2)$ $(-2.0, 0.0), (-2.0, 0.2), (0.0, -0.2)$ $(0.0, 0.2), (2.0, 0.0), (2.0, 0.2)$
z	$[0.01, 1.3]$ (step: 0.025)
T_0	$[T_{min}, T_{max}]$ (step: 1 day) $(T_{min} \text{ and } T_{max} \text{ are the min and max MJD of a season})$

Table 2: Range of the parameters used to simulate type Ia SN

2.2 Wide Fast Deep

WFD observations involve a large number of fields. The observations are dithered, and the size and depth of the final sample depends heavily on the details of the observing strategy (in particular, the filter allocation strategy and the field selection function ...) For this reason, we opted for a slightly different approach, which we describe below.

The celestial sphere is pixellized in Healpix superpixels¹. Using a simple model of the LSST focal plane, we play the cadence, and determine, the list of superpixels observed for a given exposure. This allows us to build a log which reports the mjd, band, and observing conditions of each healpixel observation.

We can then analyze this log, using as a probe, a fiducial SN Ia, e.g. the “faint” or “normal”

¹we choose $nside=64$, which corresponds to 0.8 deg^2 healpixels. We have verified that (1) larger pixels ($nside=32$) leads to underestimating the number of SNe by ~15% **recheck that** and that smaller pixels ($nside=128$ and above) give exactly the same results.

SNe Ia defined in the previous section. For each mjd and each pixel, we determine:

$$z_{\text{lim}} = \max(z | \text{LC}(z) \text{ fulfill requirements}) \quad (3)$$

$$N_{z < z_{\text{lim}}} = \delta\Omega_{\text{pix}} \int_0^{z_{\text{lim}}} \frac{\Delta T_{\text{step}}}{1+z} \mathcal{R}(z) dV(z) \quad (4)$$

where $\delta\Omega_{\text{pix}}$ is the solid angle subtended by one pixel, ΔT_{step} is the simulation time step (in observer frame days) and $\mathcal{R}(z)$ is the SN Ia volumetric rate (we adopt the rate published in (Perrett et al, 2012)). We also compute the average cadence (in day $^{-1}$), i.e. the number of g, r, i or z visits in a fiducial restframe interval.

The quantities above are determined for each pixel and each night (identified by its mjd). We report them in full sky maps, which give an assessment of how the cadence performs in a ~ 50 day time interval around the current mjd. From these maps, we can build global maps giving, as a function of the position on the sky (1) the density of supernovae (2) the median maximum redshift (3) the median cadence. We can also collate these maps in videos, that are useful to evaluate the observing strategy as a function of time.

3 Overview of observing strategies

3.1 Available strategies

Four classes of observing strategies have been studied in detail:

- the `OpSim`-based cadences released along with the white paper call (11 cadences released in June 2018 plus 4 additional simulations released in August),
- the `OpSim`- and `Feature`-based strategies that were available before the white paper call,
- simulations based on the `Altsched` scheduler proposed by Stubbs and Rothchild. This includes one rolling and another non-rolling cadence, plus a non-rolling simulation conducted on a larger footprint (P. Gris),
- finally, we have tested a series of experimental observing strategies, based on the new feature-based scheduler (a.k.a. SLAIR, Yoachim et al). These variations were produced by P. Yoachim, the main author of SLAIR, based on discussions we had at the summer 2018 DESC week (CMU) and the 2018 LSST community workshop (Tucson).

Table ?? summarizes the main characteristics of the cadences tested in this study.

As can be seen, all cadences have

3.2 Key properties

3.2.1 WFD

nb visits. n visits/night. Median internight gap. average cadence in a given time window. season duration.

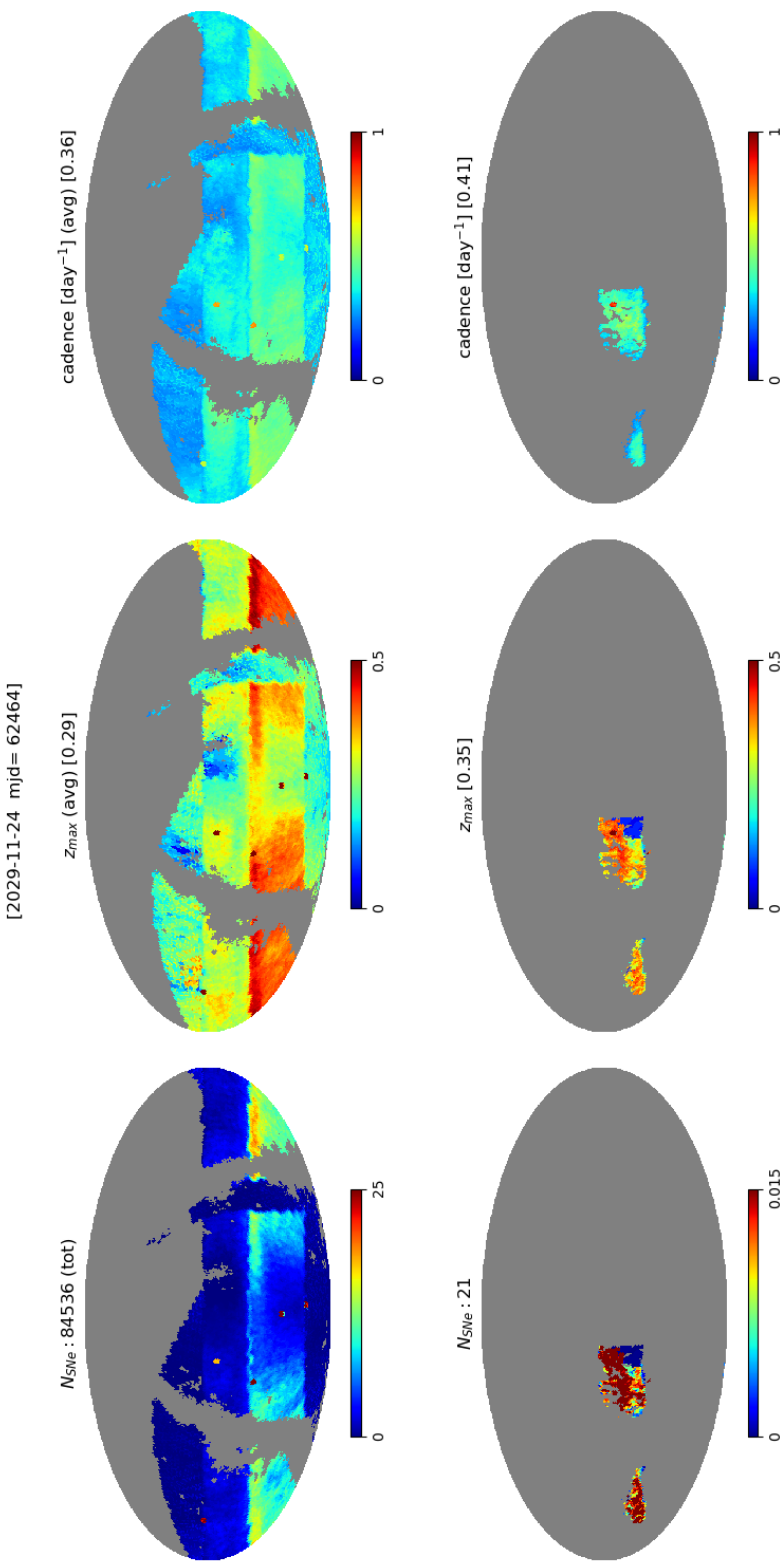


Figure 3: Example of cadence analysis maps. Cadence *Mothra_2045*, mjd=62464 (2029-11-24) *Upper panels*: (left) total number of well sampled supernovae per healpixel, (middle): median z_{med} after 2611 days of survey, (right): median cadence, after 2611 days of survey. *Lower panels*: (left) number of SNe Ia peaking at mjd=62464 and passing the light curve quality cuts (middle) z_{med} , i.e. maximum redshift at which a SN peaking at mjd=62464 would pass the requirements

1 plot that gives the average cadence vs. season duration.

Here, we show that clearly altsched dominates.

3.2.2 DDF

All proposed observing strategies but altsched-like have included DDF. Plots illustrating the four key points mentioned above are given on Figures [B1-B10](#) for baseline18a, feature_baseline_10yrs, kralen_2026 and kraken_2035 observing strategies and for the five to nine above-mentioned DDF. Among these cadences feature_baseline_10yrs displays interesting features with respect to supernovae observations for the reference DDF:

- Cadence: a median cadence of three days is observed whereas other observing strategies present cadences that may reach up to 14 days. Inter-night gaps are also smaller for COSMOS and XMM-LSS: 10 to 15 days and 5 to 7 days for the first and second maxima respectively whereas for baseline18a, kralen_2026 and kraken_2035 the first (second) maximum is at the level of 18 to 40 (13 to 20) days.
- Season length: feature_baseline_10yrs shows the highest season lengths with values around 150 days for COSMOS and XMM-LSS, and 180 days for CDFS and ELAIS-S1 whereas other strategies lead to values of about 130, 140, 120, and 150 for COSMOS, XMM-LSS, CDFS, and ELAIS-S1, respectively.
- Depth: while median m5-values are compatible among the strategies (the decrease during season 2 for the four fields in feature_baseline_10yrs is due to a known bug in the weather simulations) the coadded m5 depth per season shows clearly that feature_baseline_10yrs is a 0.7 (COSMOS), 0.4 (XMM-LSS, CDFS, ELAIS-S1) magnitude deeper (r-band) survey compared to the others. This results is to be explained by better cadences and longer seasons.

Key properties of SPT DEEP, DDF_820, DDF_858, DDF_1200 and DDF_858 fields are given on Figures [B9](#) to [B12](#).

4 Results: Number of well-measured type Ia supernovae

4.1 WFD

4.2 DD

Typical detection efficiencies are given on Fig. 6 for the COSMOS field and feature_baseline_10 yrs cadence . One may observe that the lowest efficiencies (independently on the (X_1, c) values) correspond to the first two seasons of observations which are known to be very bad for this observing strategy and for this field (see for instance Figs. [B1](#) and [B2](#)).

Efficiency curves are convolved with a production rate [1] to estimate the number of well-measured type Ia supernovae that may be collected by LSST. Summary plots are given for the

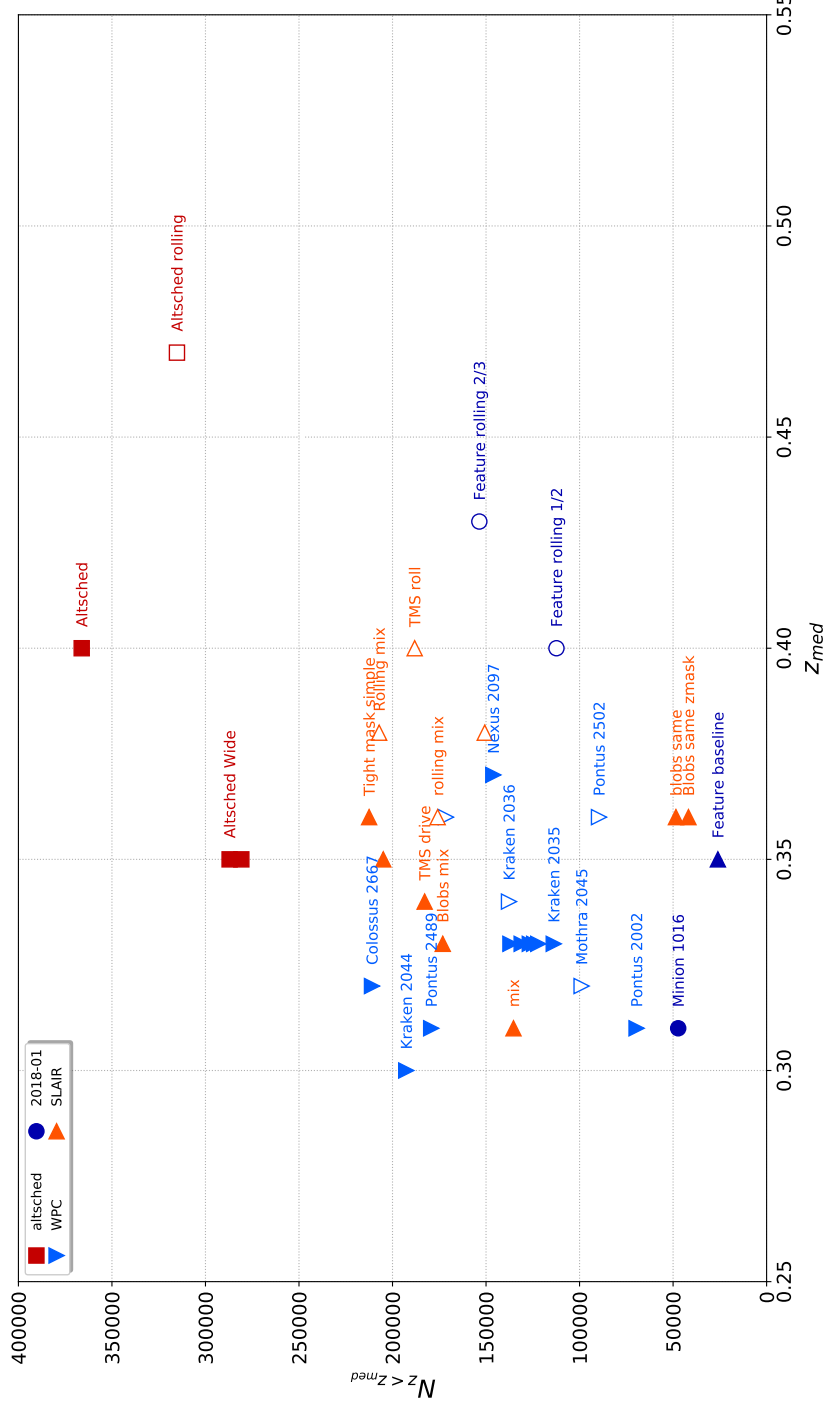


Figure 4: Representation of the cadences analyzed in this study in the plane (z_{med} , $N_{z < z_{\text{med}}}$). This gives an assessment, for each cadence, of (1) the sample depth, i.e. at which redshift the median SN no longer passes the requirements listed in section 1.1 and (2) the size of the subset of well-sampled SNe Ia.

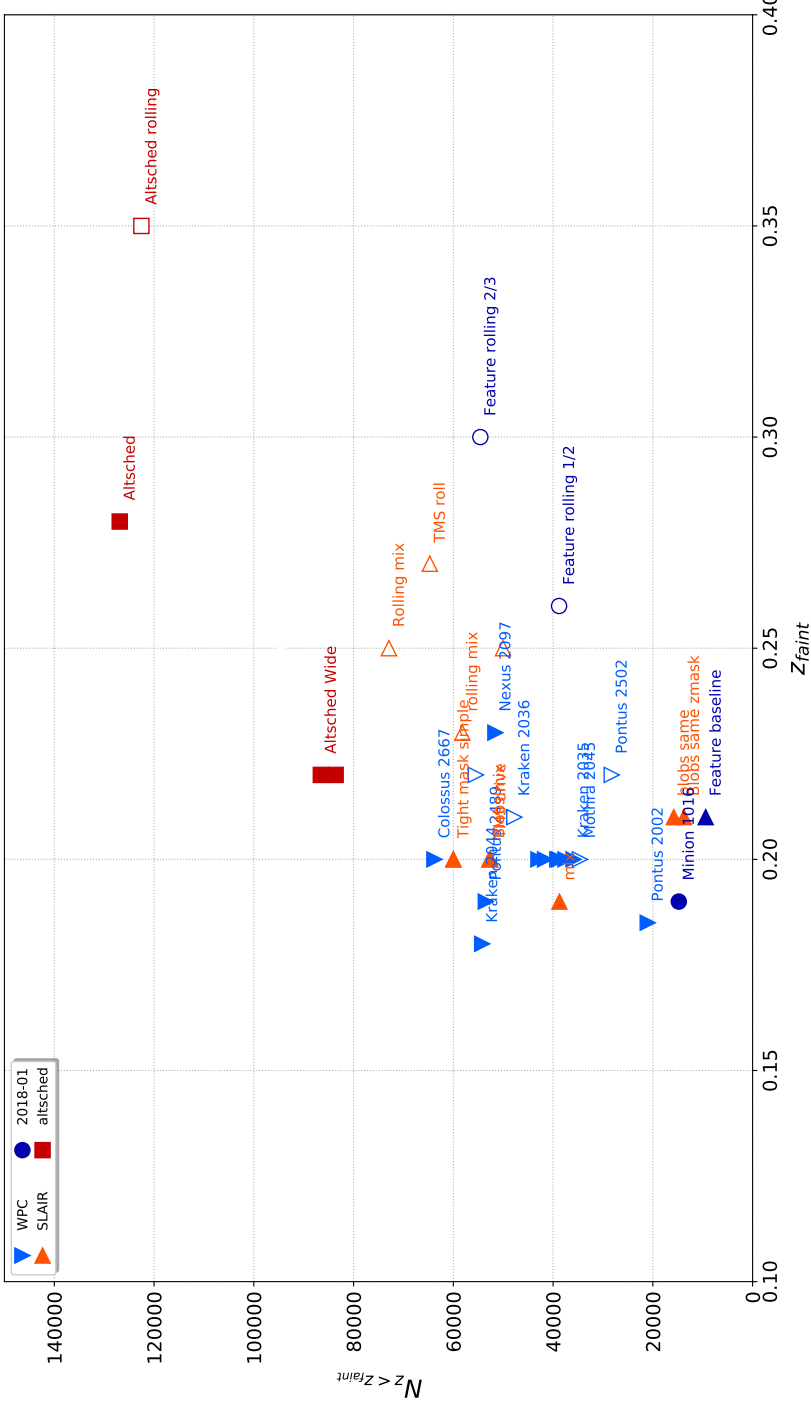


Figure 5: Representation of the cadences analyzed in this study in the plane (z_{faint} , $N_{z < z_{faint}}$). This gives an assessment, for each cadence, of (1) the redshift limit of the survey, i.e. at which redshift the faintest SN no longer passes the requirements listed in section 1.1 and (2) the size of the redshift limited SN Ia sample produced by LSST.

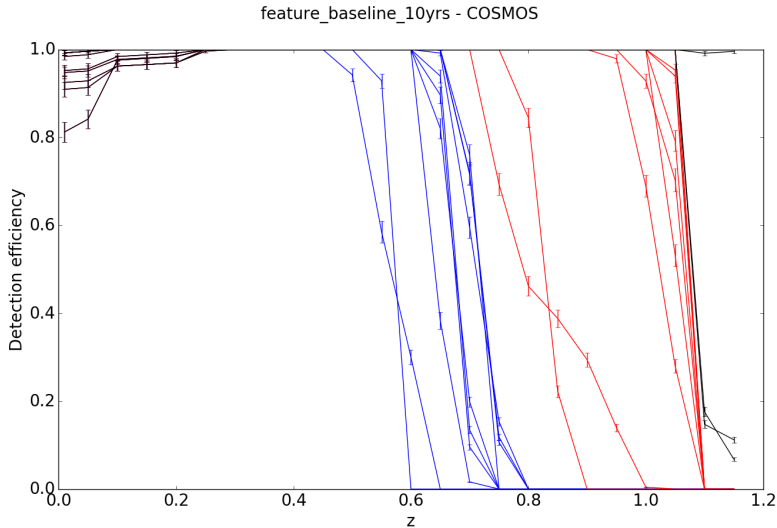


Figure 6: Detection efficiency as a function of the redshift for the COSMOS field and feature_baseline_10yrs observing strategy (10 seasons). Blue, red and black lines correspond to faint, medium and bright supernovae, respectively.

reference fields (Fig 7) and for all the DDF (Fig 8). One may observe that, despite bad observing years, feature_baseline_10yrs shows the best results in terms of number of well-measured type Ia supernovae. Equivalent results are obtained with Colossus_2667.

When considering all DDF the winner is of course kraken_2035 (27K after ten years) since this observing strategy considered 9 DDFs whereas all others observed 4 to 5 fields. One may observe that extrapolating a four fields configuration results (like the ones obtained with feature_baseline_10yrs) to a 9 DDF observing strategy will probably lead to an overestimation of the resulting number of well-measured type Ia supernovae. It is indeed difficult to maintain the same quality (in terms of cadence, season length and thus depth) when moving from a 4 to a 9 DDF strategy.

Another way to assess the quality of an observing strategy is to estimate the redshift detection limit for faint supernovae (per season and per field). On Figure 9 is displayed the 95% redshift limit (ie corresponding to the detection of 95% of the supernovae of the corresponding sample) as a function of the number of faint supernovae. Huge variations among and inside strategies are observed. This plot reflects the quality of the proposed cadences. It seems that z of 0.7-0.75 may be reached with four fields. Once again feature_baseline_10yrs tend to give the highest redshifts and the most homogeneous results among the fields and seasons.

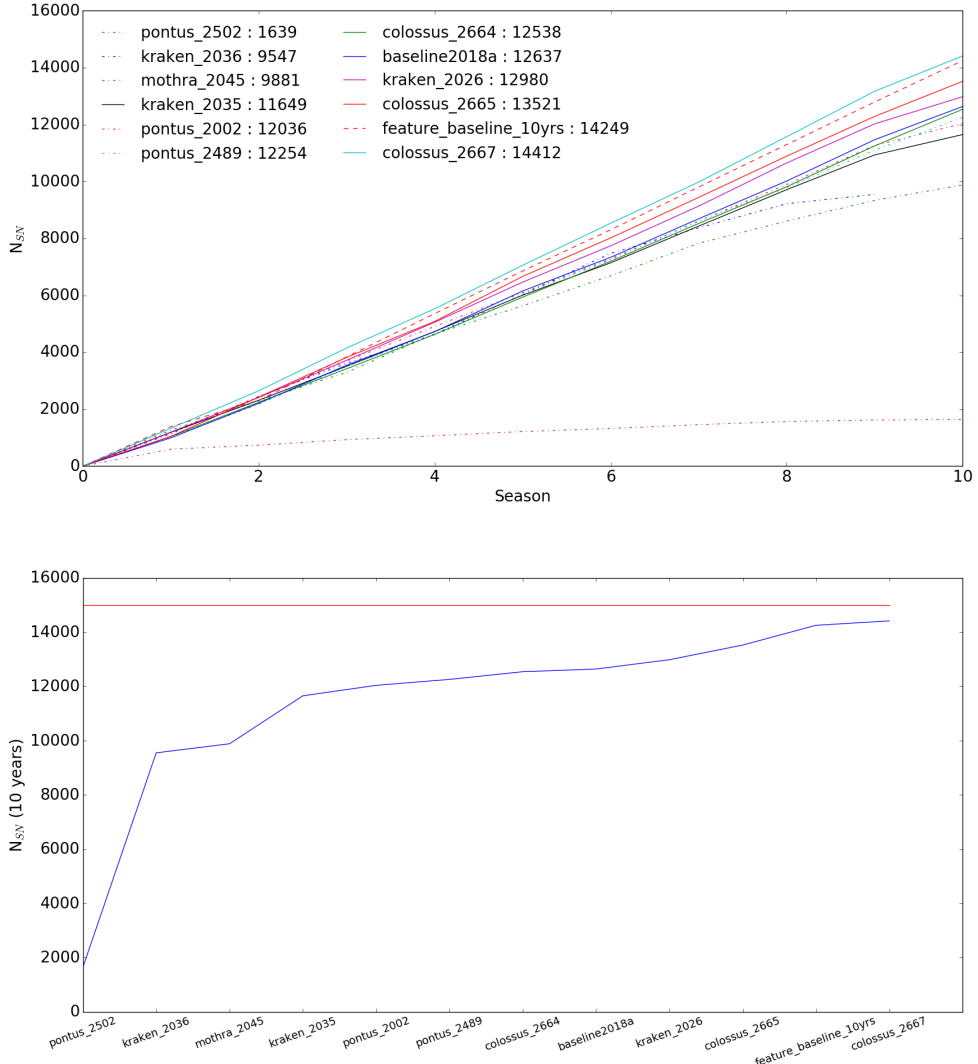


Figure 7: Top: Number of well-measured type Ia supernovae as a function of the season. Bottom: Number of well-measured type Ia supernovae as a function of observing strategy after ten years of operation. Four DDF (COSMOS,XMM-LSS,CDFS,ELAIS-S1) have been considered. The red line corresponds to 15k supernovae.

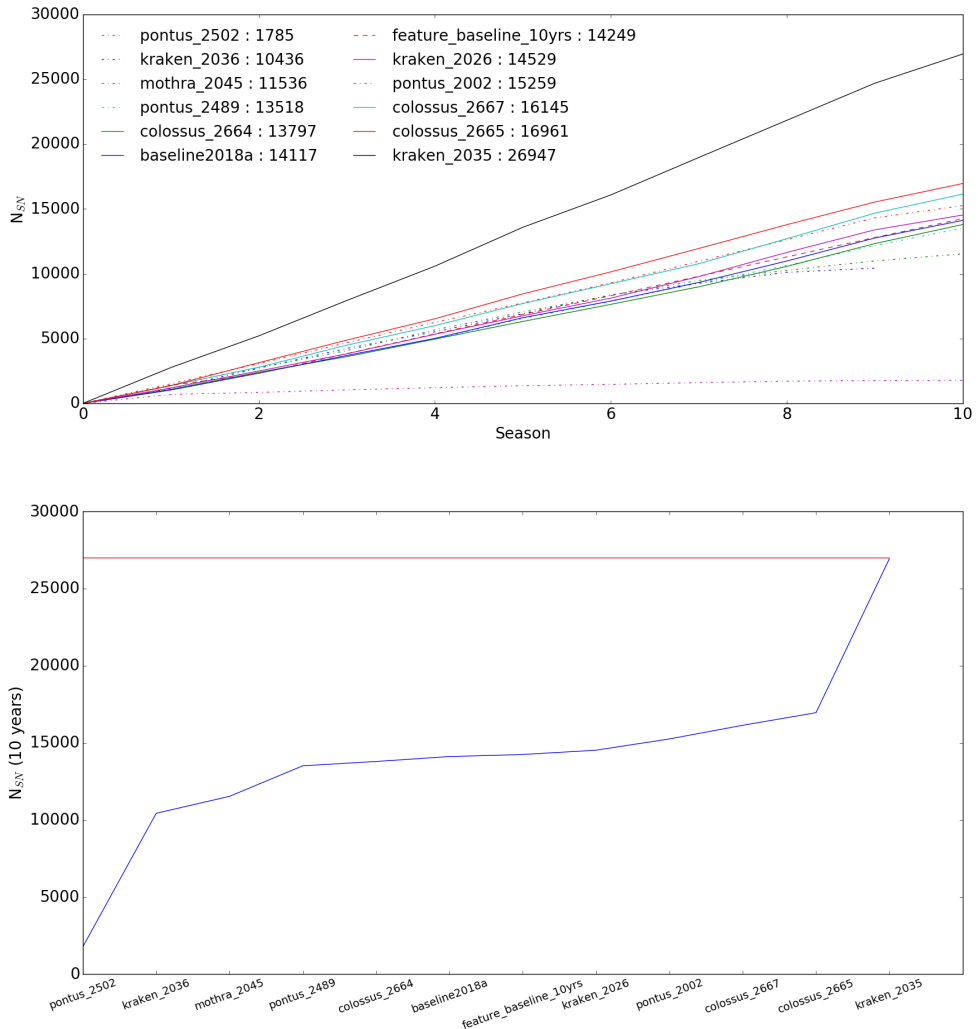


Figure 8: Top: Number of well-measured type Ia supernovae as a function of the season. Bottom: Number of well-measured type Ia supernovae as a function of observing strategy after ten years of operation. All DDF have been considered. The red line corresponds to 27k supernovae.

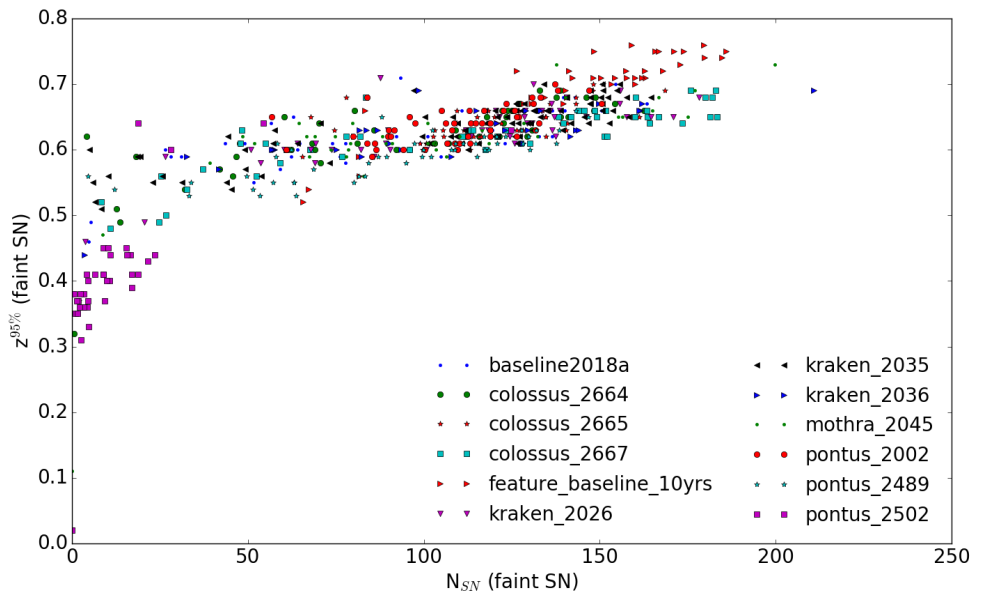


Figure 9: 95% redshift limit (ie corresponding to the detection of 95% of the supernovae of the corresponding sample) as a function of the number of faint supernovae. Each point correspond to a field, a season and an observing strategy.

5 New proposals

5.1 DDF observing strategy

In OpSim the choice to observe a given field is done on the fly according to an optimized selection function depending on criteria including (among others) observing conditions, slew time minimization, last time of visit, and total observing time. While the use of a simple metric (see below) would help in choosing another approach could be to use a pre-defined table that would specify which DDF are to be observed on a given night.

Let us consider the four reference fields COSMOS, XMM-LSS, CDFS and ELAIS-S1. Since the location are well known, it is possible to estimate when these fields are visible (that is with an altitude between 20 and 86.5 degrees) for a large enough period (typically 20 to 40 minutes) of good observing conditions (ie with airmass lower than a reference value - typically 1.5). We may define a (boolean) parameter dubbed observability equal to one when the above-mentioned conditions are filled, and 0 otherwise. This parameter is displayed on Figure 10 (top). XMM-LSS,CDFS, and ELAIS-S1 are located in the same (Ra) region and may thus be observed during the same night whereas COSMOS may be observed when all others are not visible. Season lengths of observability (Figure 10 - bottom) range from 200 to 290 days.

The table of observations may be defined using median gap values T_{gap}^{COSMOS} and T_{gap}^{others} when COSMOS and XMM-LSS,CDFS,ELAIS-S1 are not observable, respectively. Observing time windows are then defined by:

- $[T_{gap}^{others}-w/2, T_{gap}^{others}+w/2]$: COSMOS is observed
- $[T_{gap}^{COSMOS}-w, T_{gap}^{COSMOS}+w]$: XMM-LSS, CDFS, ELAIS-S1 are observed.

with a width w equal to $2/3*(T_{gap}^{COSMOS}-T_{gap}^{others})$.

5.2 altsched rolling 80/20

5.3 altsched rolling 75/25

5.4 Adding a simple metric for SN in OpSim/SLAIR

6 Conclusion

References

- [1] Evolution in the Volumetric Type Ia Supernova Rate from the Supernova Legacy Survey, K.Perrett *et al*, The Astronomical Journal, Volume 144, Issue 2 (2012).

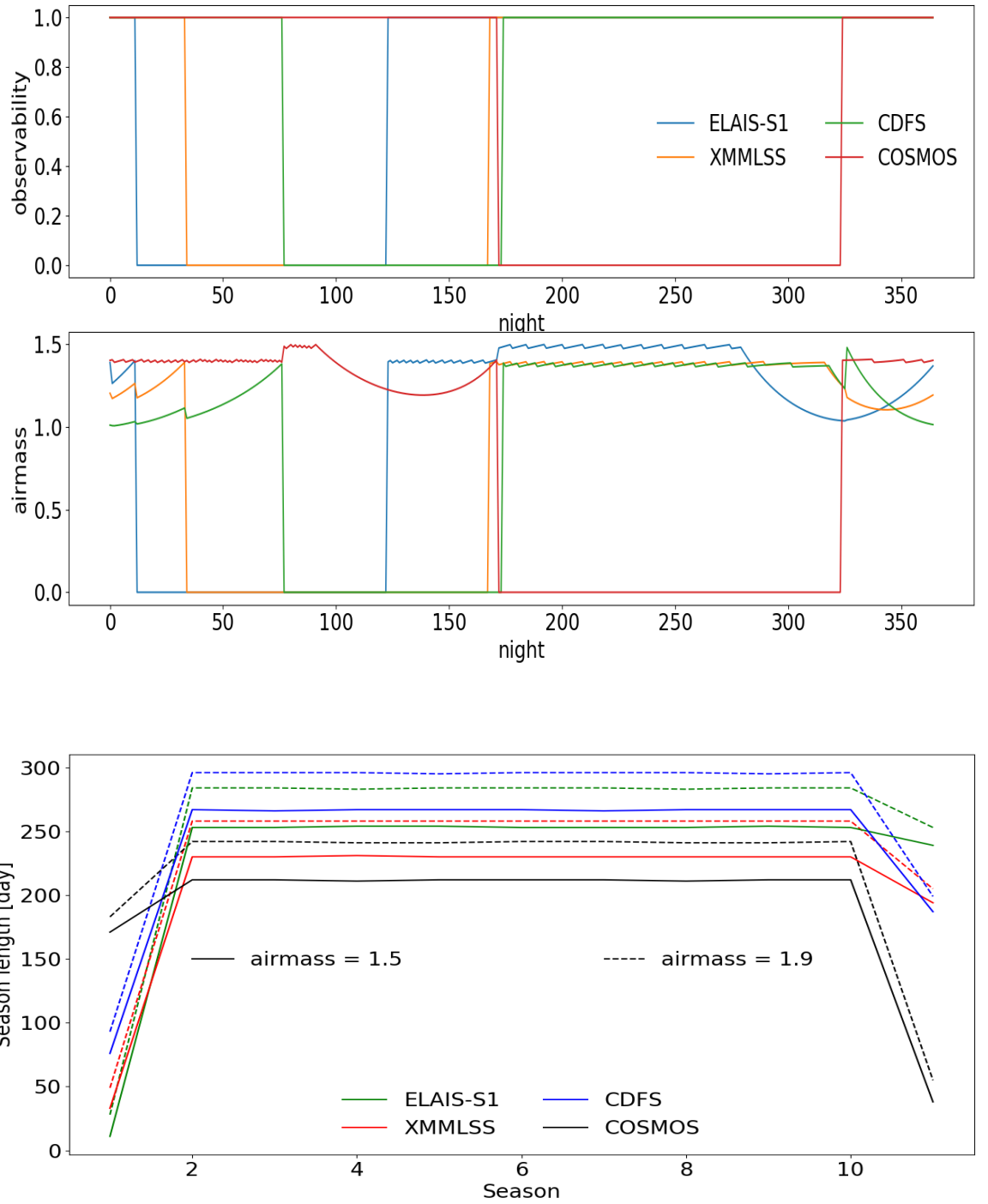


Figure 10: Top: observability (see definition in the text) and airmass as a function of the night number (first year of LSST operation). Bottom: season length as a function of the season for an airmass limit of 1.5 (full lines) and 1.9 (dashed lines).

Appendix A Derivation of formula 2

If we fit a light curve model $L(t) = A \times \ell(t)$ on a lightcurve (t_i, y_i, σ_i) , the least square estimate of A is given by:

$$\hat{A} = \frac{\sum w_i \ell_i y_i}{\sum w_i \ell_i^2}$$

and the signal-to-noise ratio on \hat{A} is:

$$SNR = \sum_i (w_i L_i^2)^{1/2}$$

since we are in the background dominated regime, the weights may be expressed as a function of the $5 - \sigma$ limiting flux of each visit $f_{i|5}$, and we have:

$$SNR_{\text{band}} = \sum_i 5 \times (f_{i|5}^{-2} L_i^2)^{1/2}$$

where $5 - \sigma$ limiting flux of each visit $f_{i|5}$.

Appendix B DDF plots

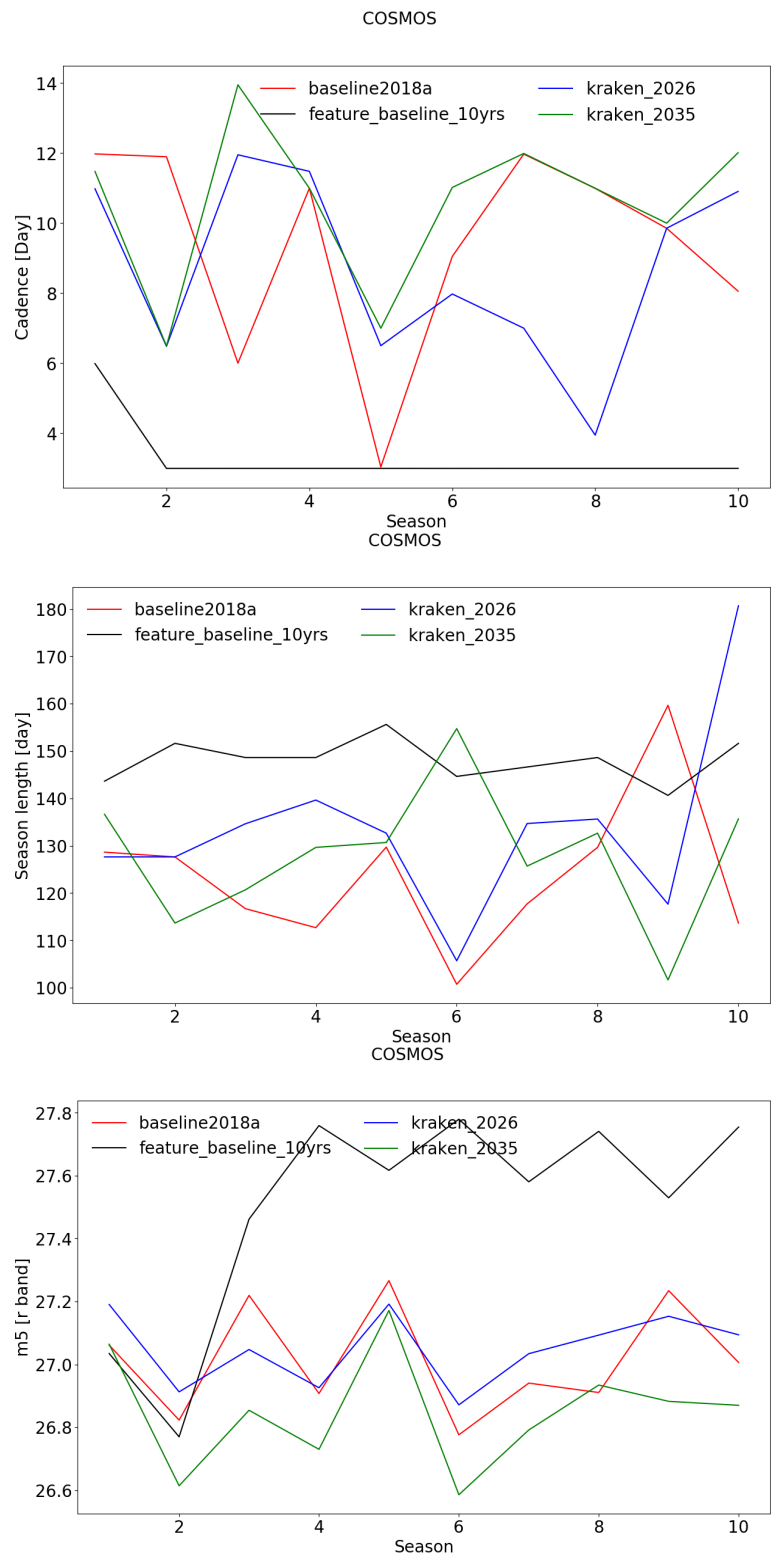


Figure B1: Cadence (top, in day), season length (middle, in day) and coadded m_5 (bottom, in mag) as a function of the season for the COSMOS field and baseline18a, feature_baseline_10yrs, kraken_2026 and kraken_2035 observing strategies.

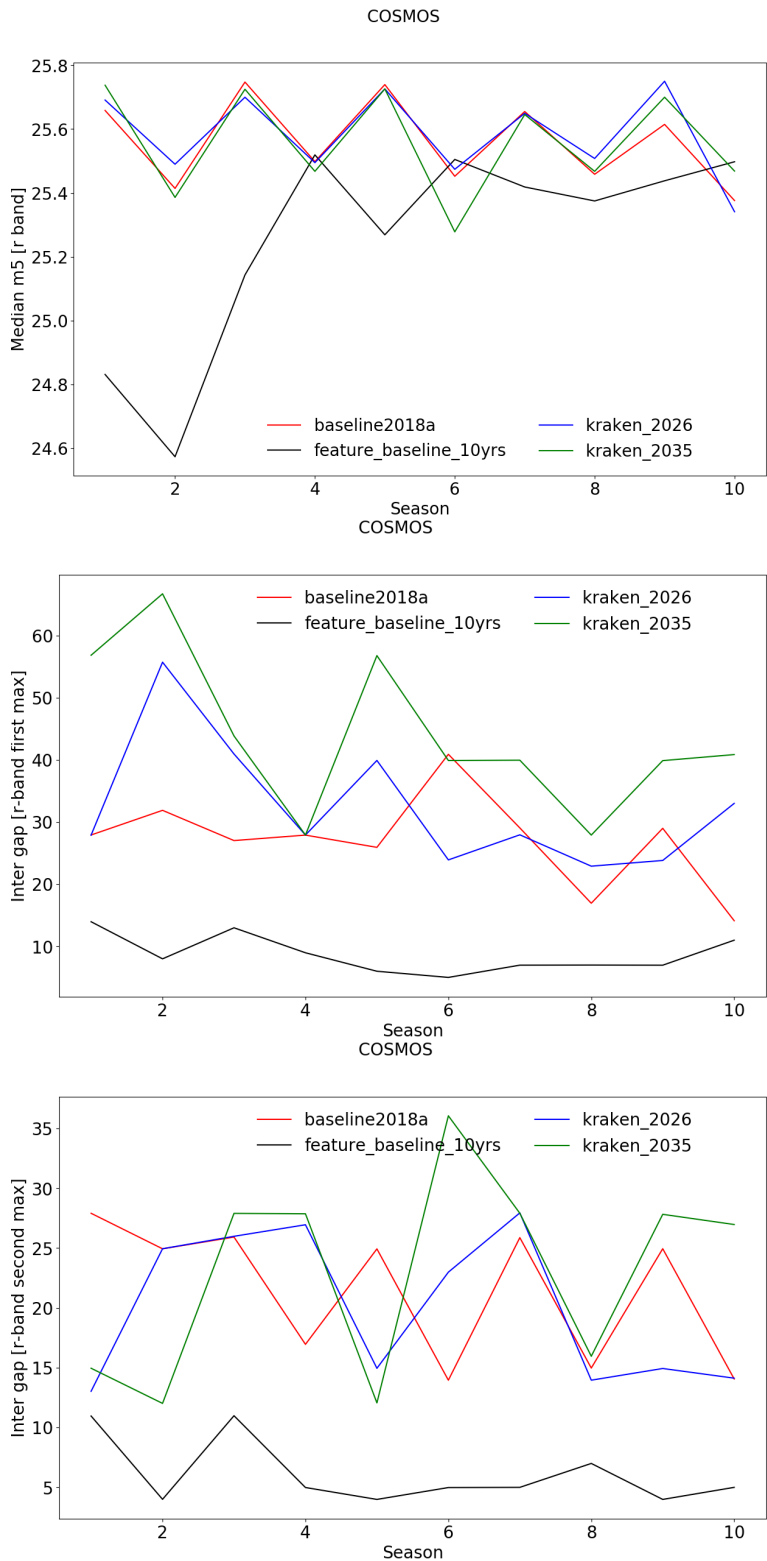


Figure B2: Median m5 (top, in mag), first maximum inter-night gap (middle, in day) and second maximum inter-night gap (bottom, in day) as a function of the season for the COSMOS field and baseline18a, feature_baseline_10yrs, kraken_2026 and kraken_2035 observing strategies.

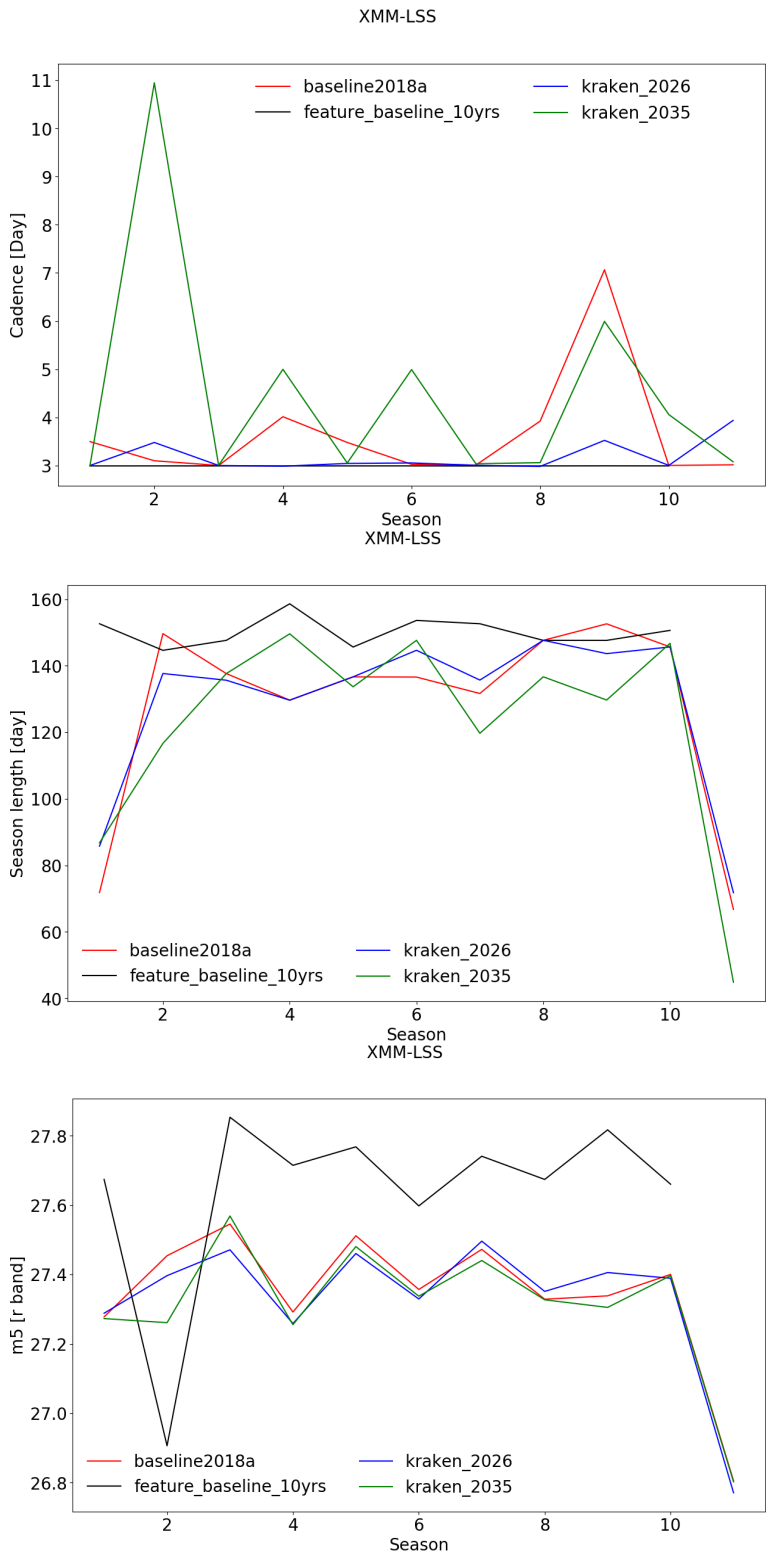


Figure B3: Cadence (top, in day), season length (middle, in day) and coadded $m5$ (bottom, in mag) as a function of the season for the XMM-LSS field and baseline18a, feature_baseline_10yrs, kraken_2026 and kraken_2035 observing strategies.

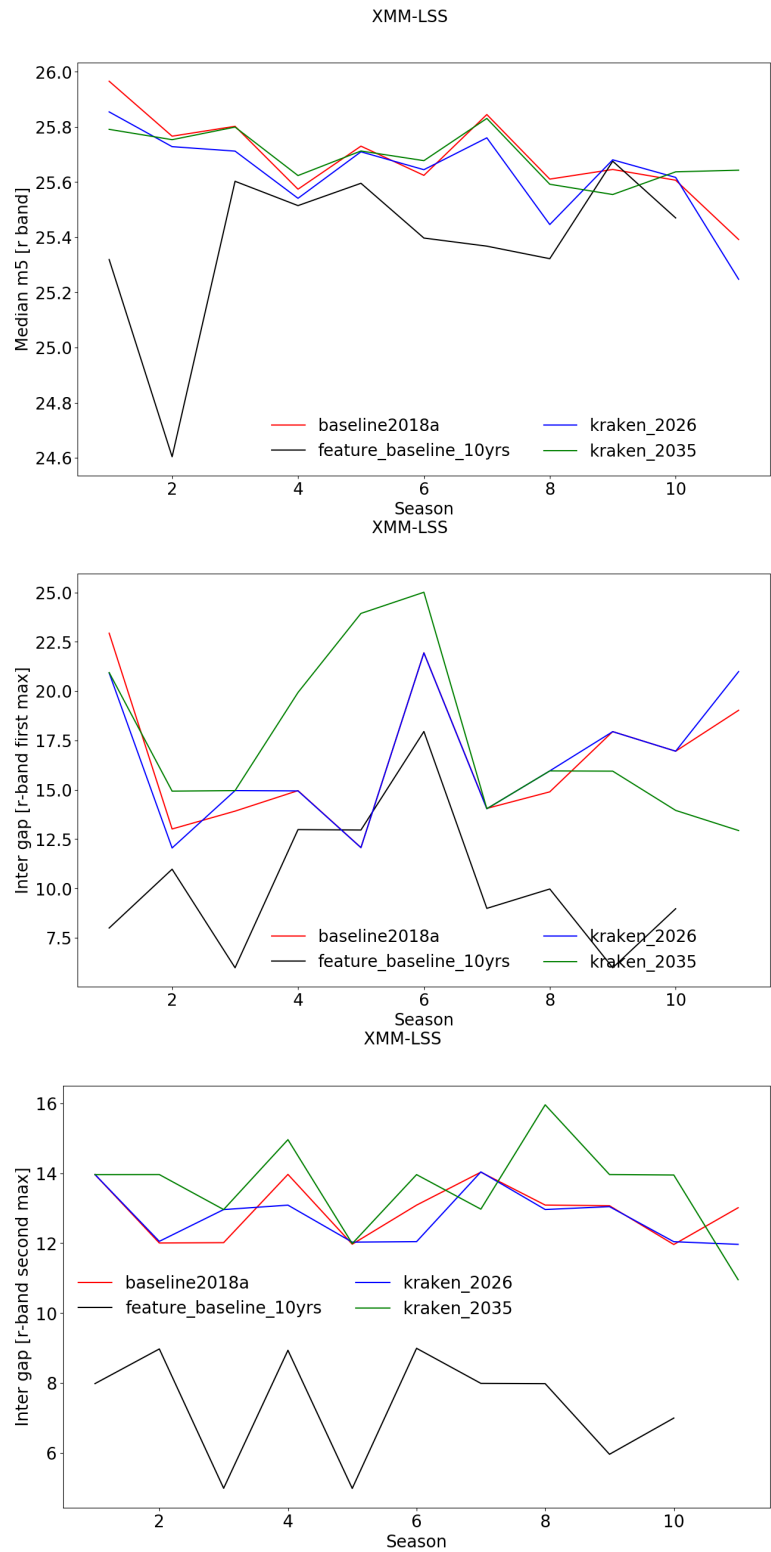


Figure B4: Median m5 (top, in mag), first maximum inter-night gap (middle, in day) and second maximum inter-night gap (bottom, in day) as a function of the season for the XMM-LSS field and baseline18a, feature_baseline_10yrs, kraken_2026 and kraken_2035 observing strategies.

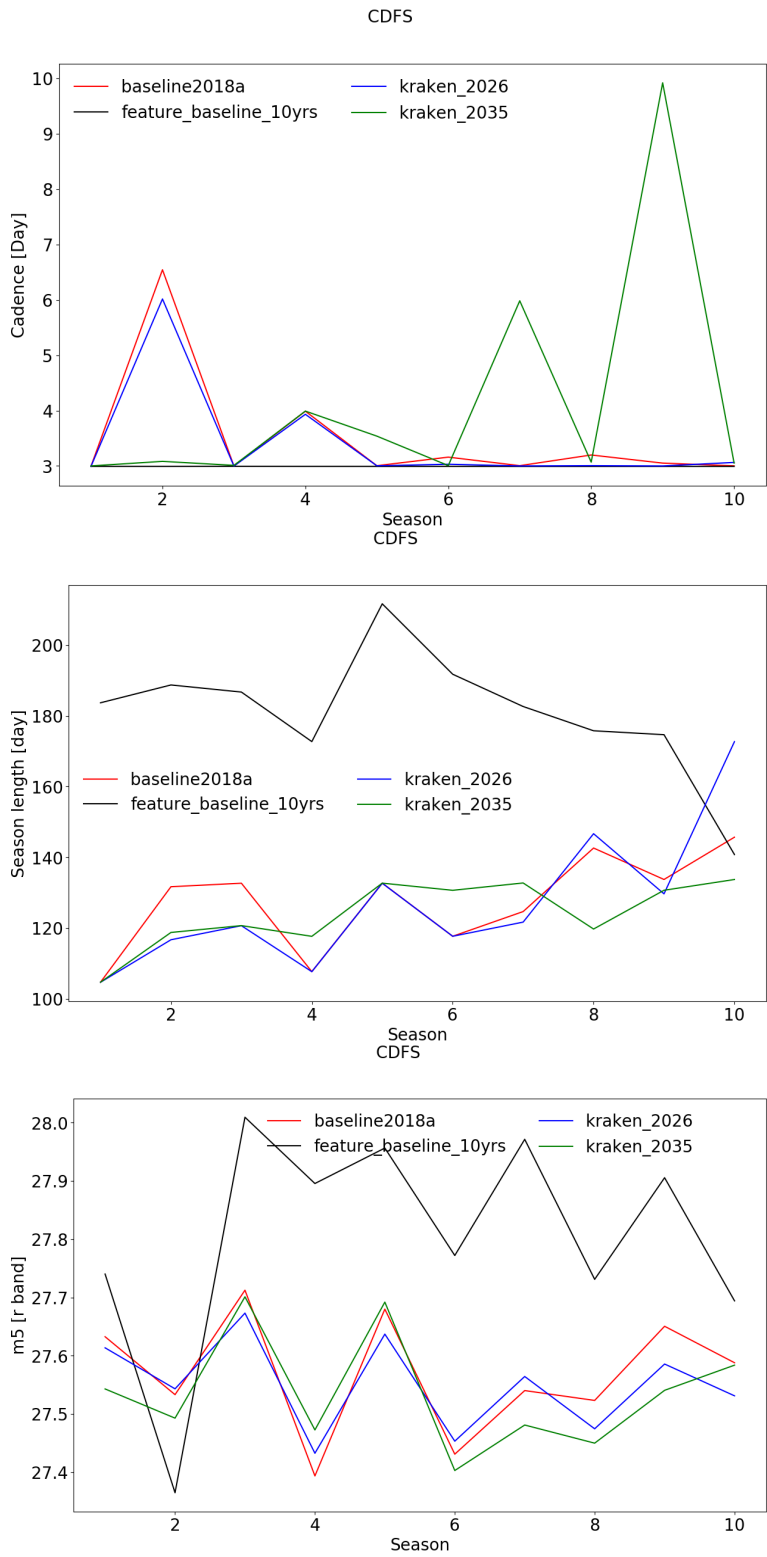


Figure B5: Cadence (top, in day), season length (middle, in day) and coadded $m5$ (bottom, in mag) as a function of the season for the CDFS field and baseline18a, feature_baseline_10yrs, kraken_2026 and kraken_2035 observing strategies.

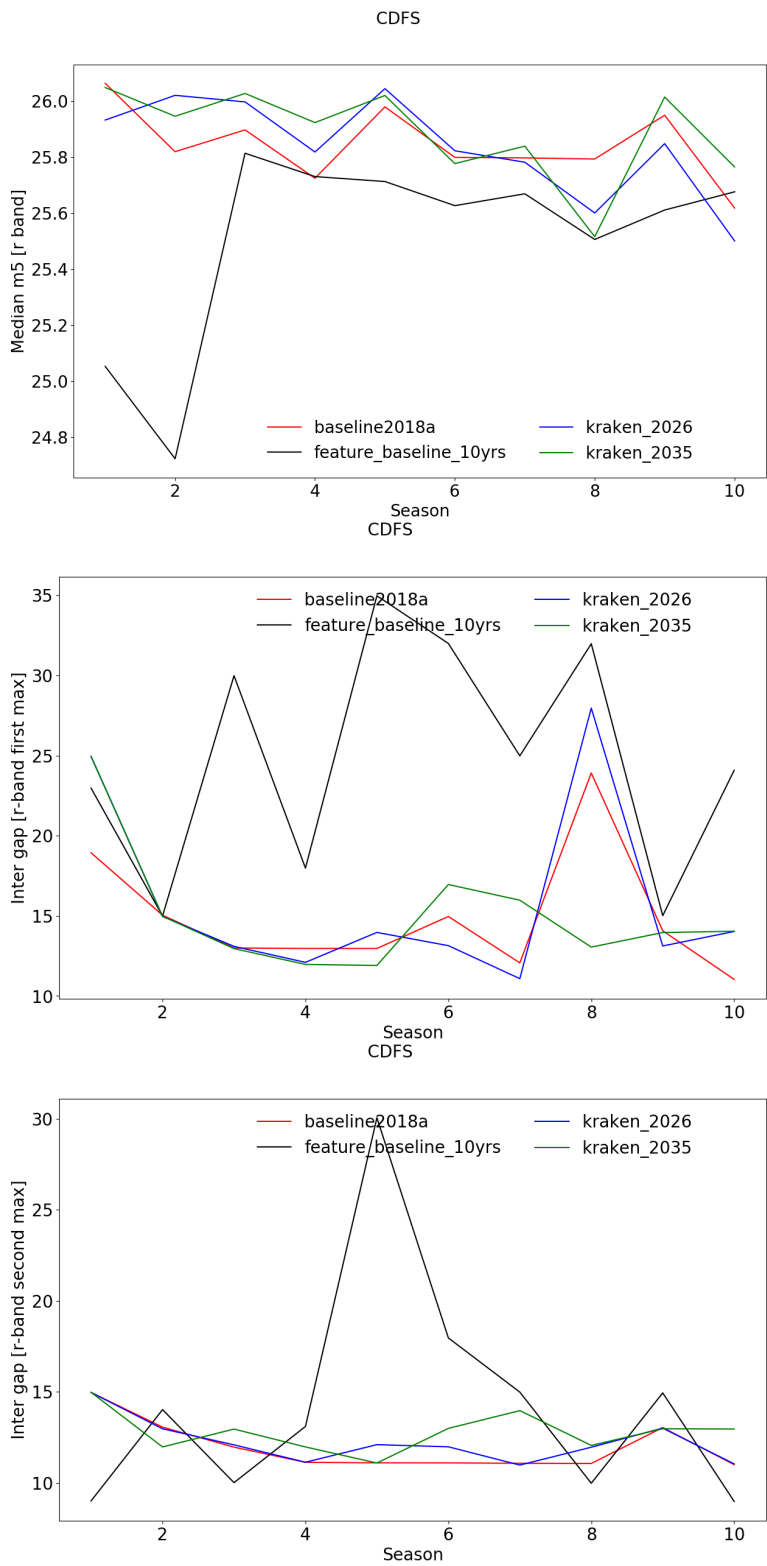


Figure B6: Median m5 (top, in mag), first maximum inter-night gap (middle, in day) and second maximum inter-night gap (bottom, in day) as a function of the season for the CDFS field and baseline18a, feature_baseline_10yrs, kraken_2026 and kraken_2035 observing strategies.

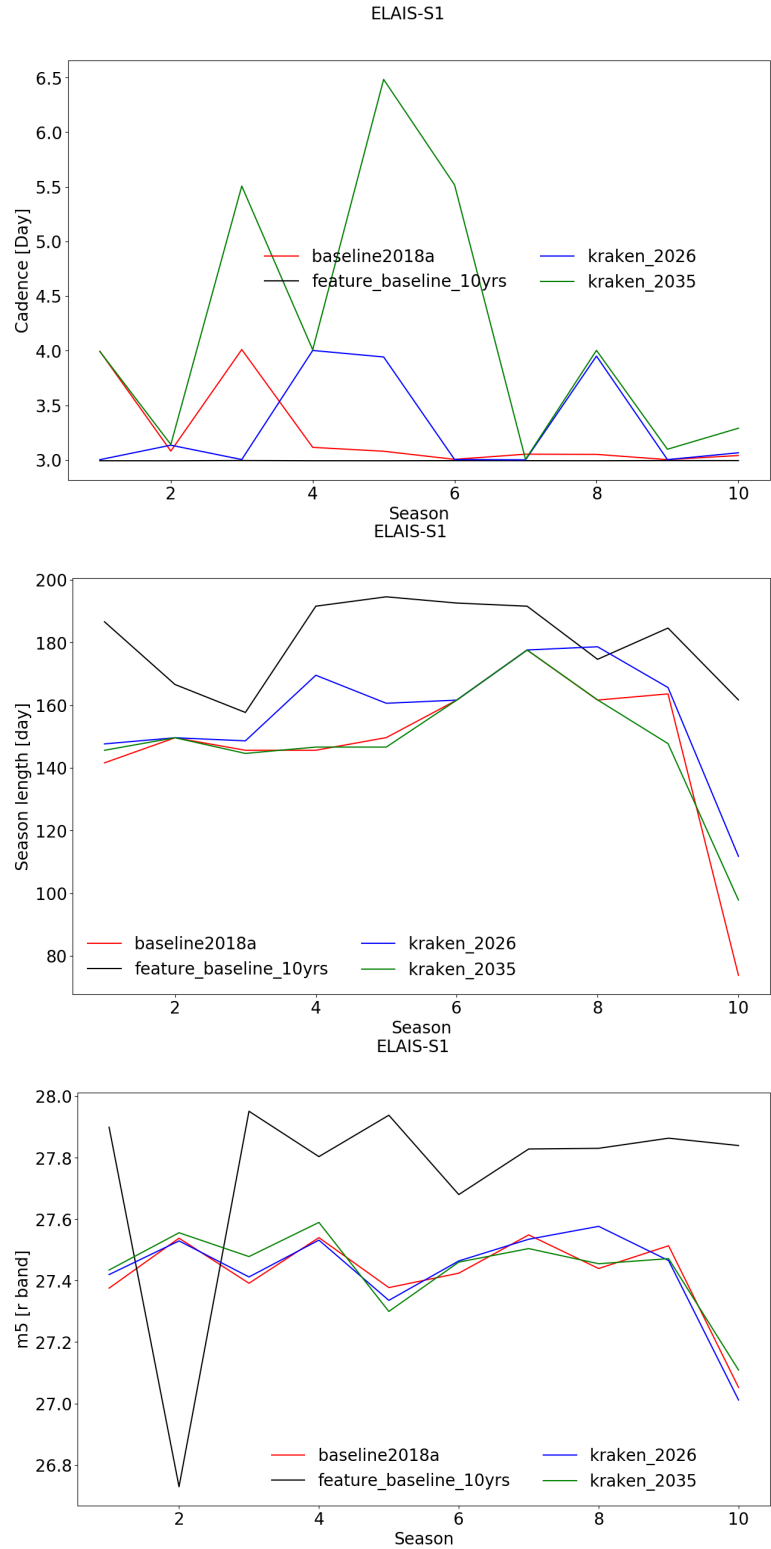


Figure B7: Cadence (top, in day), season length (middle, in day) and coadded $m5$ (bottom, in mag) as a function of the season for the ELAIS-S1 field and baseline18a, feature_baseline_10yrs, kraken_2026 and kraken_2035 observing strategies.

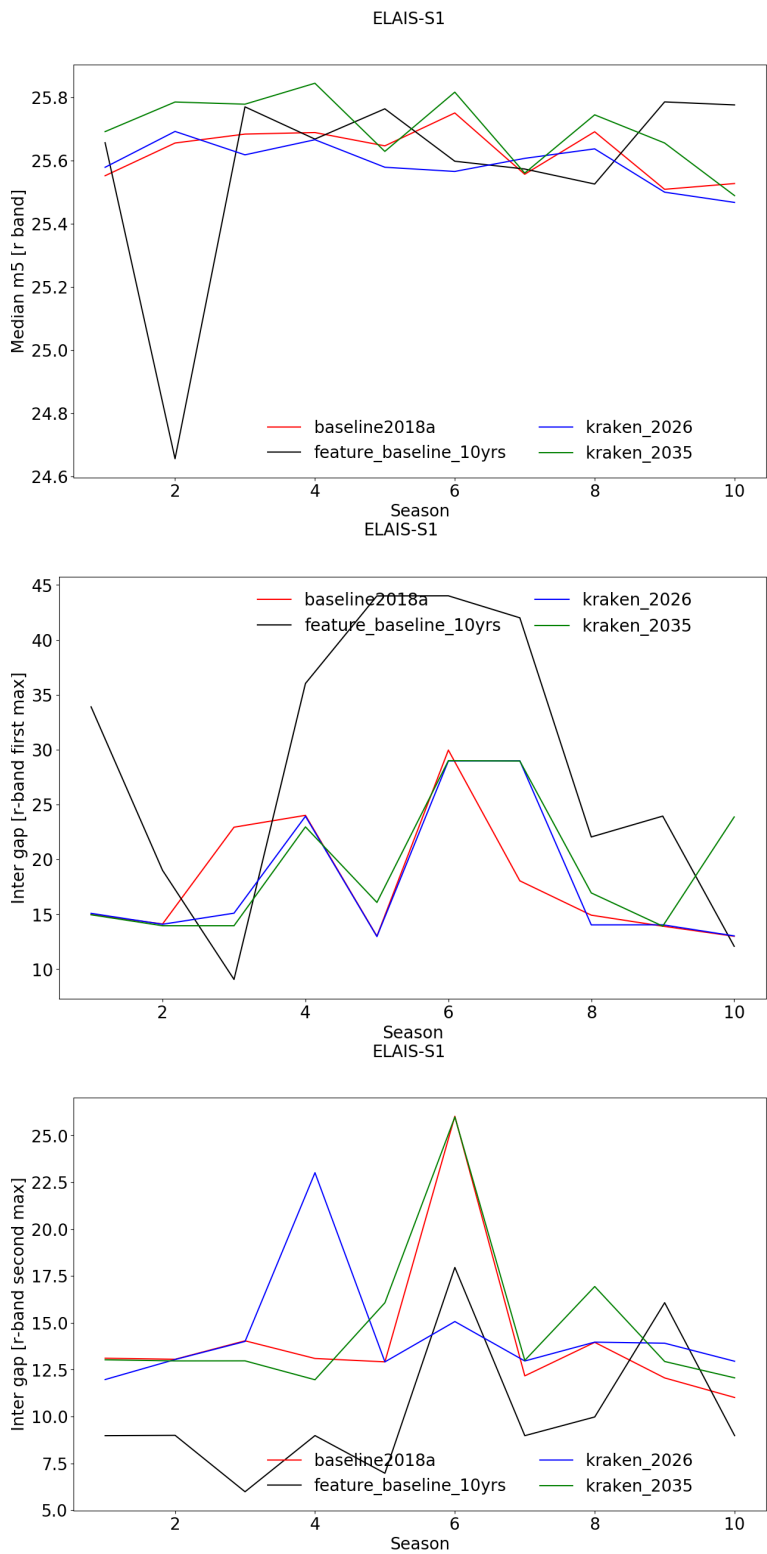


Figure B8: Median m5 (top, in mag), first maximum inter-night gap (middle, in day) and second maximum inter-night gap (bottom, in day) as a function of the season for the ELAIS-S1 field and baseline18a, feature_baseline_10yrs, kraken_2026 and kraken_2035 observing strategies.

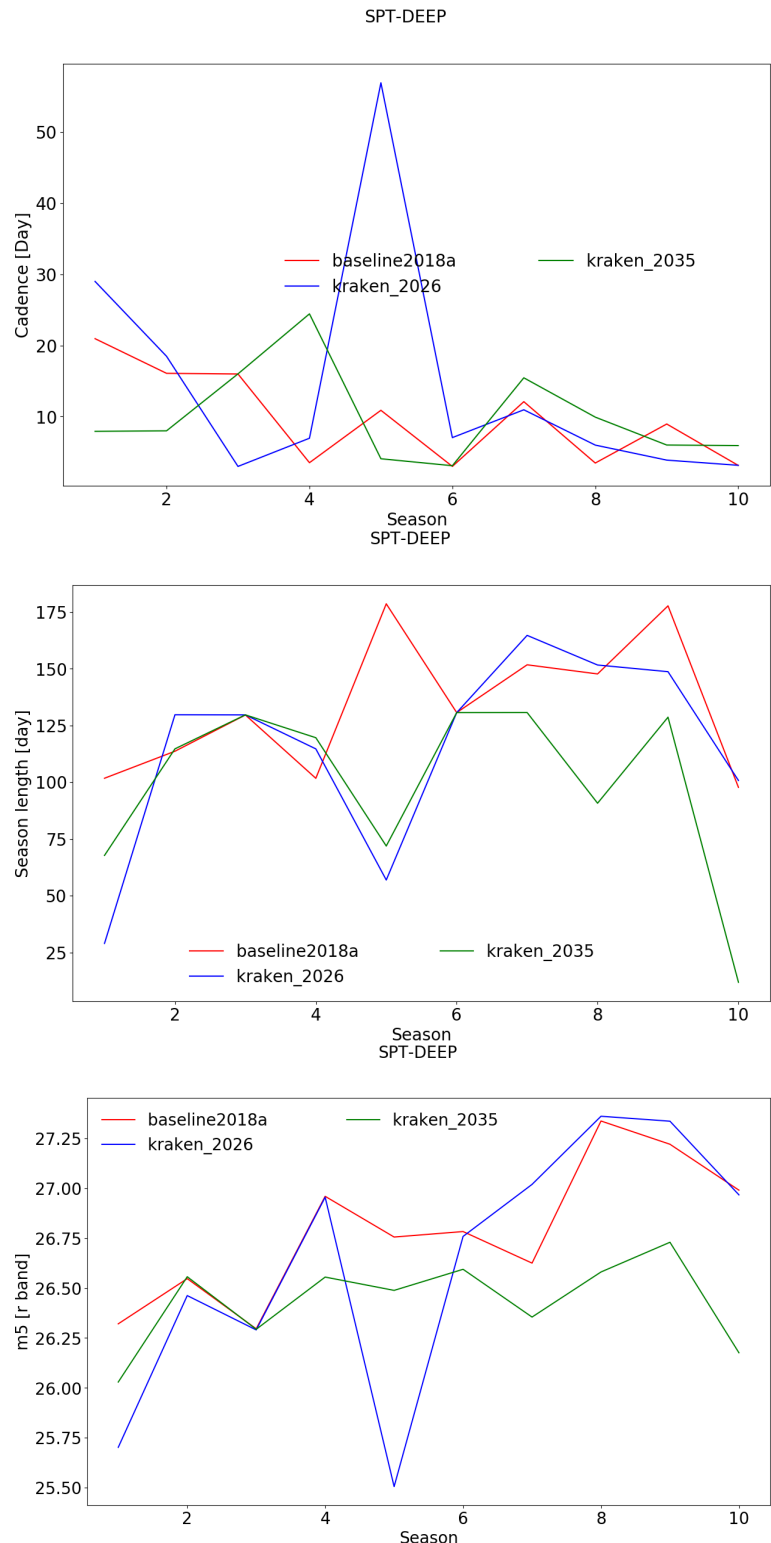


Figure B9: Cadence (top, in day), season length (middle, in day) and coadded m5 (bottom, in mag) as a function of the season for the SPT DEEP field and baseline18a, feature_baseline_10yrs, kraken_2026 and kraken_2035 observing strategies.

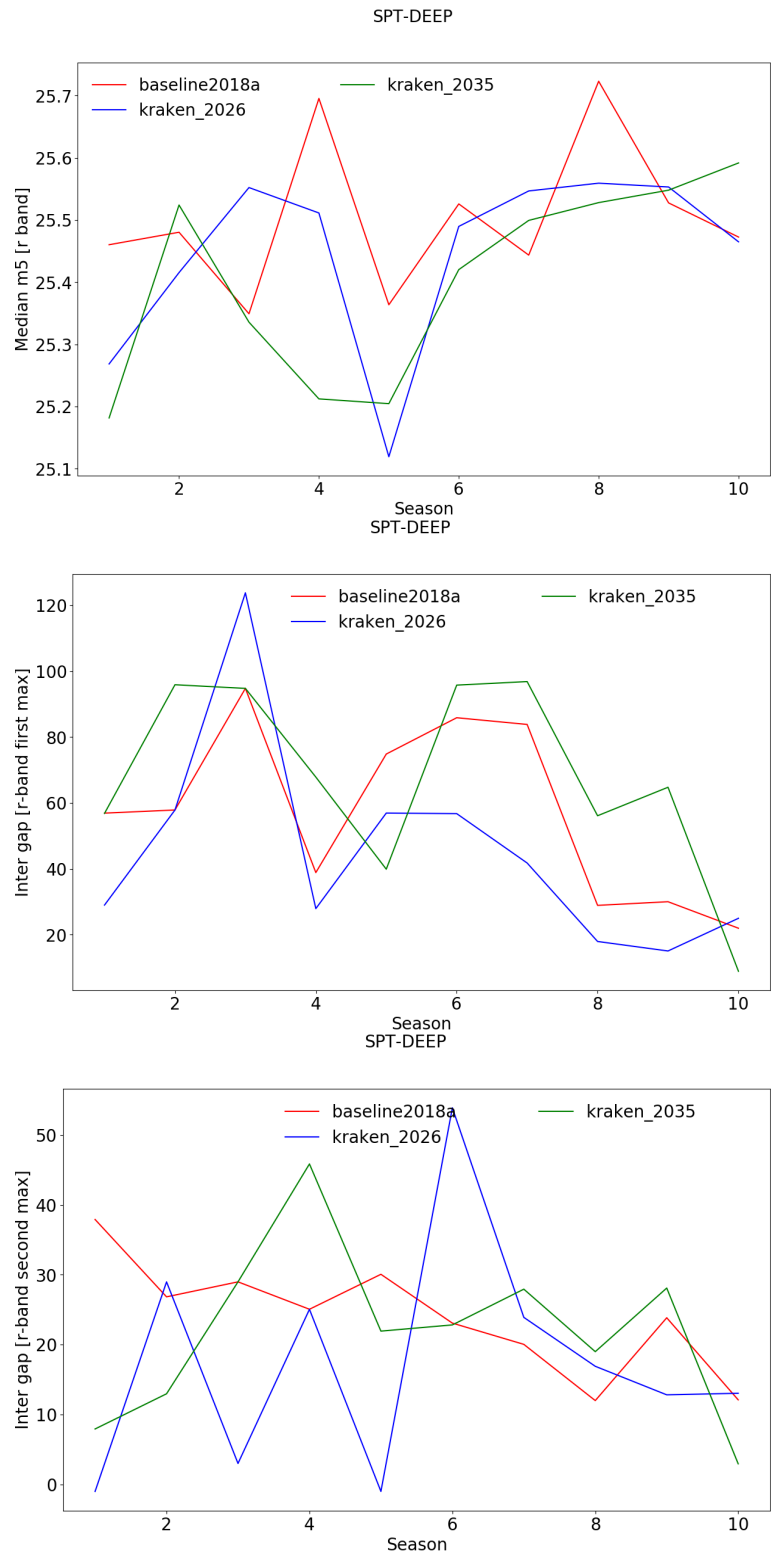


Figure B10: Median m5 (top, in mag), first maximum inter-night gap (middle, in day) and second maximum inter-night gap (bottom, in day) as a function of the season for the SPT DEEP field and baseline18a, feature_baseline_10yrs, kraken_2026 and kraken_2035 observing strategies.

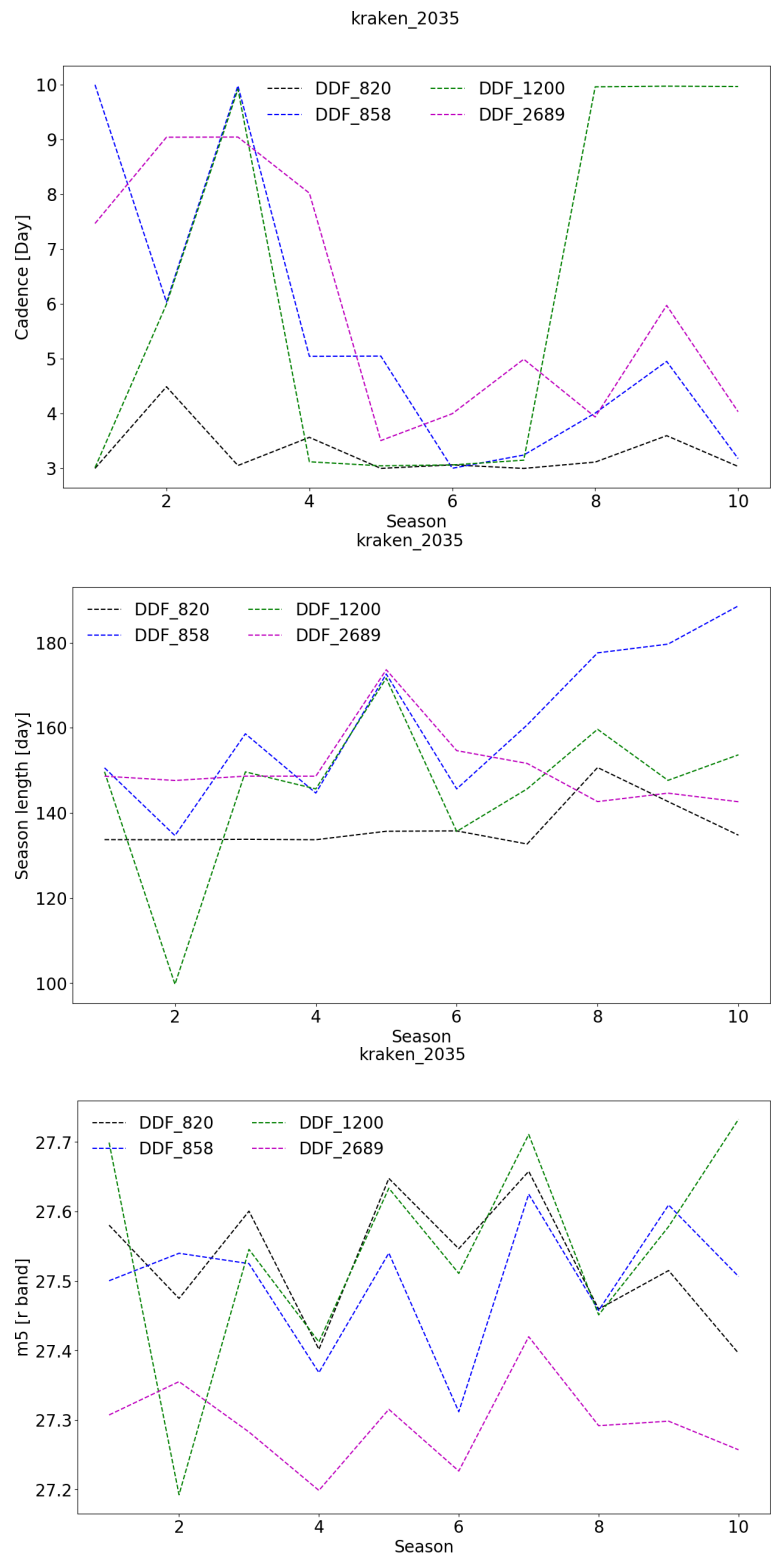


Figure B11: Cadence (top, in day), season length (middle, in day) and coadded $m5$ (bottom, in mag) as a function of the season for DDF_820, DDF_858, DDF_858and DDF_2689fields and kraken_2035 observing strategy.
 30
 30

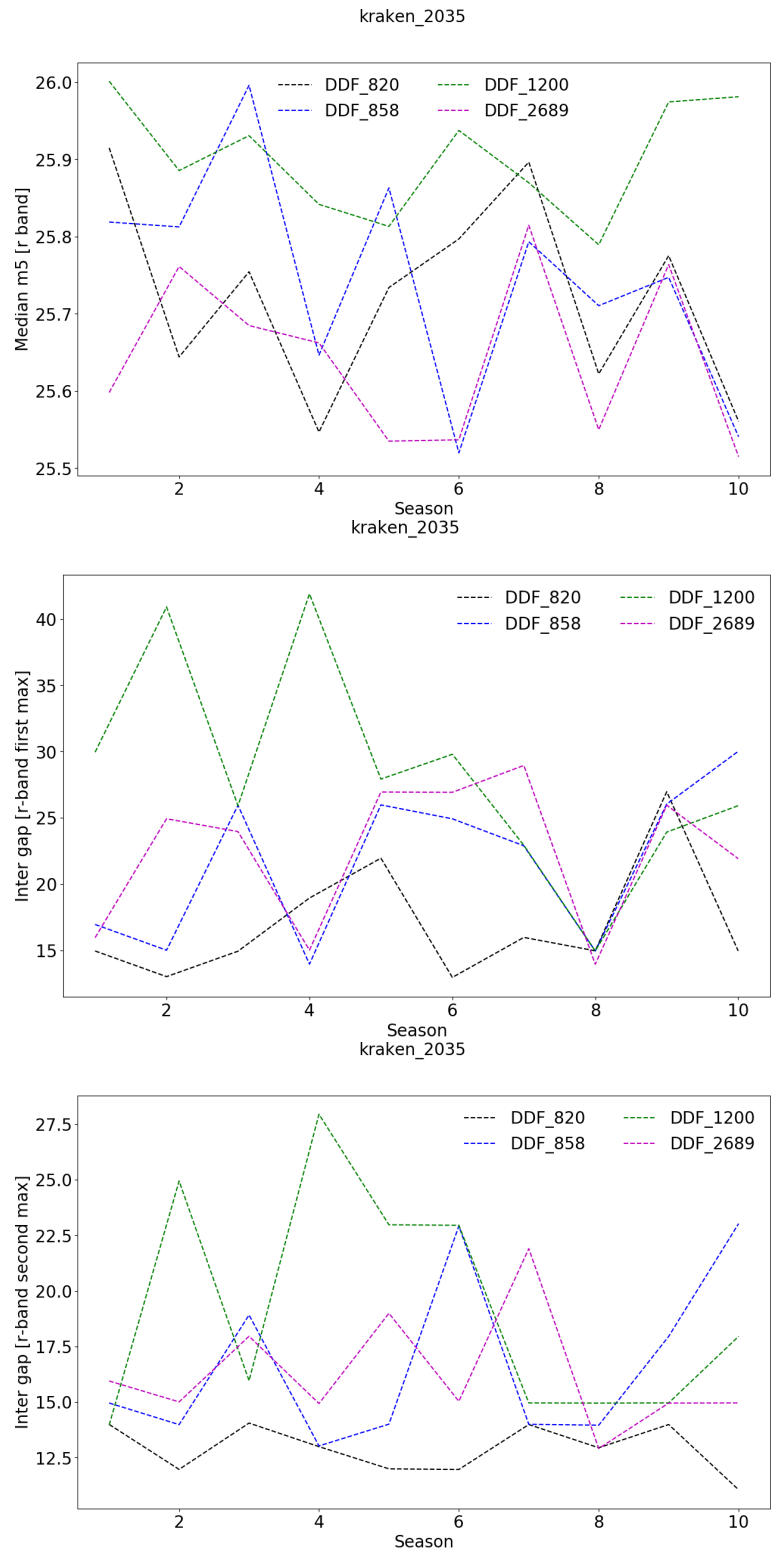


Figure B12: Median m5 (top, in mag), first maximum inter-night gap (middle, in day) and second maximum inter-night gap (bottom, in day) as a function of the season for DDF_820, DDF_858, DDF_858 and DDF_2689 fields and kraken_2035 observing strategy.